Modeling and Analysis of Crosstalk for Time-Interleaved Photonic ADCs

Cheng Wang, Guiling Wu, Zhengtao Jin, and Jianping Chen

***Abstract*—We build a model of channel response for time-interleaved photonic analog-to-digital converters (TIPADCs) including interchannel and intrachannel crosstalks. The characteristic of the channel magnitude responses of TIPADCs in the cases with and without mismatch are analyzed under different backend bandwidths. When a backend bandwidth is less than half of the overall sampling rate, interchannel crosstalk will cause a periodical variation on the corresponding channel magnitude response in mismatch-free TIPADCs, with the period being the overall sampling rate. The periodicity caused by interchannel crosstalk will be disrupted by time mismatch in TIPADCs. The theoretical analyses are verified by the simulation results of 2- and 4-channel TIPADCs and experimental measurements of a 2-channel TIPADC system.**

***Index Terms*—Crosstalk, mismatch, channel response.**

I. Introduction

PHOTONIC analog-to-digital converters have the potential of improving the performance of electronic analog-to-digital converters (EADCs) [1]–[4]. TIPADCs have attracted many attentions since they can reach high sampling rate and lower the requirement for the electrical backend by adopting wavelength division multiplexing and/or time division multiplexing method [2]. In TIPADCs, however, limited isolation among channels in wavelength division multiplexers (WDMs) or time division multiplexers (TDMs) and backend electrical bandwidth in practice would result in interchannel and intrachannel crosstalks, respectively. Williamson *et al.* analyzed the error of recovered signal caused by the crosstalk occurring in demultiplexers after the electro-optic modulator (EOM) and predicted the frequency response of corresponding interleaving spurs [5]. K. Furusawa *et al.* intuitively analyzed the temporal and spectral crosstalk caused by WDMs in TIPADCs and their requirements on the spectral width and repetition rate of light sources [6]. F. Su *et al.* analyzed the effect of intrachannel crosstalk on channel response [7]. However, the effect of interchannel crosstalk and the combined effect of two kinds of crosstalks on the sampling result/output of TIPADCs have not been investigated. The effect of crosstalk on the sampling result/output of TIPADCs is still an open problem.

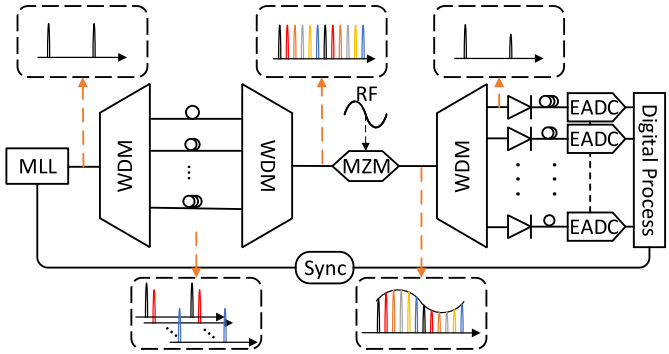

Fig. 1. The diagram of TIPADCs.

In this paper, we build a channel response model including crosstalks for TIPADCs and analyze the effects of crosstalks on system channel responses in the cases with and without mismatch, respectively. When a mismatch-free TIPADC has a backend bandwidth less than half of the overall sampling rate, interchannel crosstalk will result in a periodical variation on the corresponding channel magnitude response, with the period being the overall sampling rate. For a TIPADC with mismatches, time mismatch will result in the loss of the periodicity. The upper limits for crosstalk and time mismatch are discussed relative to quantization noise. 2- and 4-channel TIPADCs with different backend bandwidths are simulated, and a 2-channel TIPADC is experimentally measured in terms of their channel magnitude responses. According to the model and results, one can analyze whether a TIPADC is affected by crosstalks and which kinds of crosstalk is the main limiting factor. The model and results can also be applied to optimize the design of TIPADCs in terms of mitigating the effect of crosstalks.

II. Modeling of Channel Response With Crosstalks

Fig. 1 illustrates a typical structure of a TIPADC [2], [6]–[10]. A mode-locked laser (MLL) generates an optical pulse train with a broad spectrum and a repetition rate of f_s. The optical pulse train is sliced by a WDM to produce N sub-trains to N channels. Corresponding time delays are introduced into the transmission of the sub-trains, which combine to form a pulse train with a higher repetition rate of Nf_s. A Mach-Zehnder modulator (MZM) is applied to modulate the optical pulse train with an RF

Manuscript received September 24, 2019; revised December 25, 2019 and March 2, 2020; accepted March 28, 2020. Date of publication April 3, 2020; date of current version July 23, 2020. This work was supported by the National Natural Science Foundation of China under Grant 61535006 and Grant 61627817. *(Corresponding author: Guiling Wu.)*

The authors are with the State Key Laboratory of Advanced Optical Communication Systems and Networks, Shanghai Institute for Advanced Communication and Data Science, Department of Electronic Engineering, Shanghai Jiao Tong University, Shanghai 200240, China (e-mail: wang_cheng@sjtu.edu.cn; wuguiling@sjtu.edu.cn; vincary@sjtu.edu.cn; jpchen62@sjtu.edu.cn).

Color versions of one or more of the figures in this article are available online at http://ieeexplore.ieee.org.

Digital Object Identifier 10.1109/JLT.2020.2984811

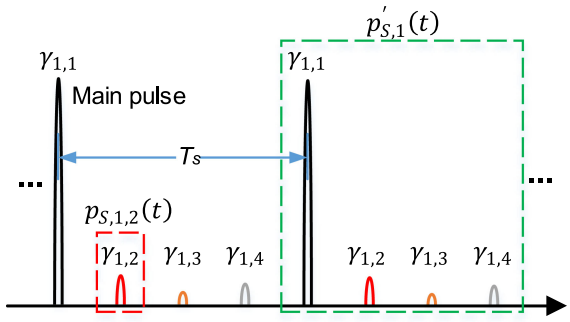

Fig. 2. The pulse train of channel 1 after demultiplexing with interchannel crosstalk.

signal. The modulated pulse train is then distributed by a WDM into N channels to be digitized by EADCs, respectively.

Fig. 2 illustrates the pulse train of channel 1 for a 4-channel system with interchannel crosstalk, which can be expressed as:

$$p_{n,crstk}(t) = P_{A,n}\sum_{m=1}^{N}\gamma_{n,m}\sum_{k=-\infty}^{\infty}p_{S,n,m}\left(t-kT_s-d_{P,m}\right) = P_{A,n}\sum_{k=-\infty}^{\infty}p'_{S,n}\left(t-kT_s\right), \quad (1)$$

where $P_{A,n}$ is the average power of the main pulse train of channel n. $\gamma_{n,m}$ is the ratio of the pulse power crosstalking from channel m to channel n, to the power of the main pulse train in channel n. $p_{S,n,m}(t)$ is the temporal shape of a pulse crosstalking from channel m to channel n, and $d_{P,m}$ is the optical time delay of channel m relative to channel 1. $T_s = 1/f_s$. Denoting $p'_{S,n}(t) = \sum_{m=1}^{N}\gamma_{n,m}p_{S,n,m}(t-d_{P,m})$, which is a set of consecutive pulses repeating every T_s in channel n.

Due to the characteristic of the MZM, the digitized output signal of channel n is composed of an unmodulated part and a modulated part [7], [11]. The unmodulated part can be expressed as:

$$v_{Q0,n}[i] = \frac{1}{2}\alpha p_{n,crstk}(t) * h_{E,n}(t-d_{E,n})\Big|_{t=iT_s} = \frac{1}{2}\alpha\int_{-\infty}^{\infty}p_{n,crstk}(-\tau)h_{E,n}(\tau-d_{E,n})d\tau, \quad (2)$$

where α is the attenuation factor of the MZM to the pulse train, $h_{E,n}(t)$ represents the impulse response of backend electrical devices, and $d_{E,n}$ is the electrical delay of channel n. It can be seen that $v_{Q0,n}[i]$ is a DC component which is irrelevant to t and RF signal, and does not affect the system frequency response.

Considering the modulated part, denoted as $v_{Q1,n}[i]$, we have:

$$v_{Q1,n}[i] = h_{A,n}(t) * v_I(t)|_{t=iT_s}, \quad (3)$$

where $v_I(t)$ is the RF signal and $h_{A,n}(t)$ is the equivalent impulse response of channel n. From [7], the equivalent impulse response of channel n, denoted as $h_{A,n}(t)$, is derived as:

$$h_{A,n}(t) = -\frac{1}{2}\alpha h_M(t) * \left[p_{n,crstk}(-t)h_{E,n}(t-d_{E,n})\right], \quad (4)$$

where $h_M(t)$ is the small-signal impulse response of the MZM. Thus $h_{A,n}(t)$ depends on the product of $h_{E,n}(t-d_{E,n})$ and $p_{n,crstk}(-t)$ within the bandwidth of the MZM.

The Fourier transform of $h_{A,n}(t)$ is denoted as $H_{A,n}(\Omega)$ and can be derived as (detailed in appendix):

$$H_{A,n}(\Omega) = -\frac{\alpha P_{A,n}}{2T_s}H_M(\Omega) \times \sum_{k=-\infty}^{\infty}P'_{S,n}(k\Omega_s)H'_{E,n}(\Omega+k\Omega_s), \quad (5)$$

where $P'_{S,n}(\Omega) = \sum_{m=1}^{N}\gamma_{n,m}P_{S,n,m}(\Omega)e^{-j\Omega d_{P,m}}$ is the Fourier transform of $p'_{S,n}(t)$, $P_{S,n,m}(\Omega)$ is the Fourier transform of $p_{S,n,m}(t)$, and $H'_{E,n}(\Omega) = H_{E,n}(\Omega)e^{-j\Omega d_{E,n}}$.

When the bandwidths of $P_{S,n,m}(\Omega)$ are much broader than that of $H'_{E,n}(\Omega)$, which is satisfied in most practical PADC cases, the filtering effect of pulse shape can be ignored. In the case, the temporal shapes of all pulses in channel n can be considered approximately the same and denoted as $p_S(t)$. Thus $P'_{S,n}(\Omega)$ can be simplified as:

$$P'_{S,n}(\Omega) = P_S(\Omega)\sum_{m=1}^{N}\gamma_{n,m}e^{-j\Omega d_{P,n}} = P_S(\Omega)\Gamma_n(\Omega), \quad (6)$$

where $P_S(\Omega)$ is the Fourier transform of $p_S(t)$, and $\Gamma_n(\Omega) = \sum_{m=1}^{N}\gamma_{n,m}e^{-j\Omega d_{P,m}}$.

If there is no interchannel crosstalk, which corresponds to:

$$\gamma_{n,m} = \begin{cases}1, & \text{if and only if } \ m=n\\ 0, & \text{others}\end{cases}, \quad (7)$$

then (4) degenerates into:

$$h_{A,n}(t) = -\frac{1}{2}\alpha P_{A,n}h_M(t) * \left[h_{E,n}(t-d_{E,n}) \times \sum_{k=-\infty}^{\infty}p_S(t-kT_s+d_{P,n})\right], \quad (8)$$

which is the same as that in [7].

A. Channel Response Without Channel Mismatch

When relative optical time delays between channels are ideal, i.e., $d_{p,m} = (m-1)T_s/N$, we have:

$$\begin{cases}|\Gamma_n(k\Omega_s)| = |\Gamma_n(k\Omega_s + N\Omega_s)| \leqslant \Gamma_n(0)\\ \arg[\Gamma_n(k\Omega_s)] = \arg[\Gamma_n(k\Omega_s + N\Omega_s)]\\ \arg[\Gamma_n(0)] = \arg[\Gamma_n(N\Omega_s)] = 0.\end{cases} \quad (9)$$

Equation (9) shows that both the magnitude and the phase of $\Gamma_n(k\Omega_s)$ ($|\Gamma_n(k\Omega_s)|$, $\arg[\Gamma_n(k\Omega_s)]$) have a periodicity of $N\Omega_s$, and reach max values and zero at $kN\Omega_s$, respectively, as shown in Fig. 3(a) and (b). According to (6), $|P'_{S,n}(k\Omega_s)|$ is illustrated in Fig. 3(c). When $P_S(\Omega)$ has a zero-phase in our system, the phase response of $P'_{S,n}(\Omega)$ is the same as $\arg[\Gamma_n(\Omega)]$.

According to (5), within the bandwidth of $H_M(\Omega)$, $H_{A,n}(\Omega)$ is the sum of shifting $H'_{E,n}(\Omega)$ with different weights of

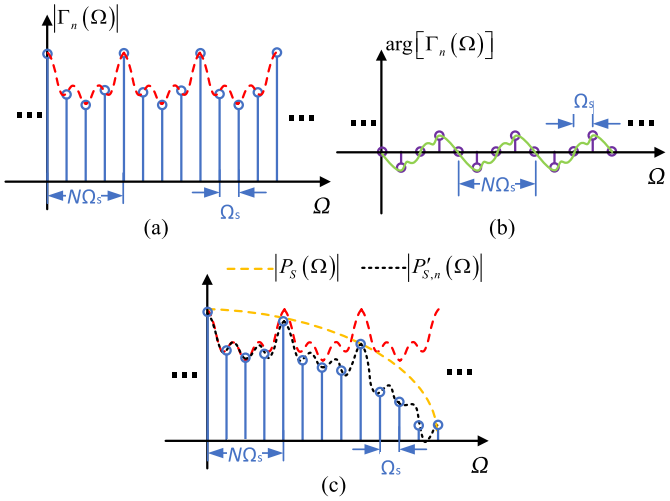

Fig. 3. Illustration of (a) $|\Gamma_n(k\Omega_s)|$, (b) $\arg[\Gamma_n(k\Omega_s)]$, (c) $|P'_{S,n}(k\Omega_s)|$.

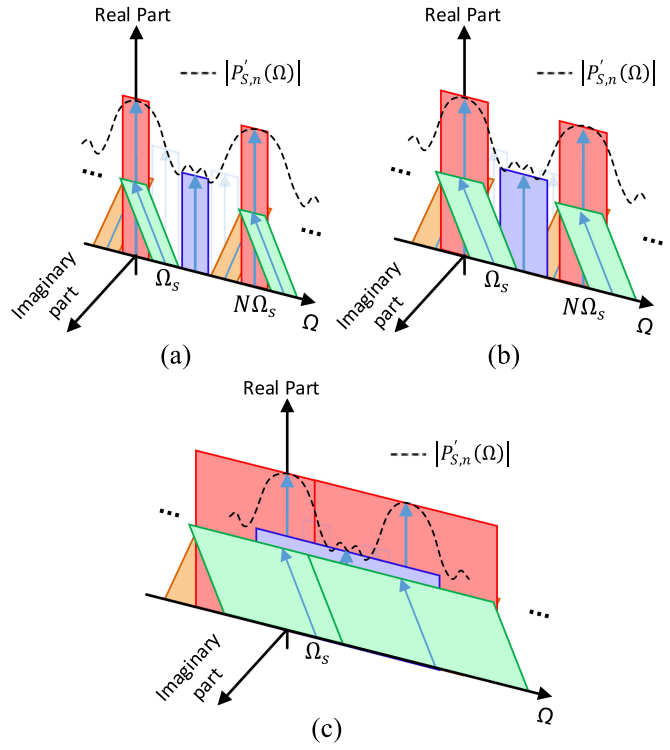

Fig. 4. $H_{A,n}(\Omega)$ for (a) $B_{E,n} < \Omega_s/2$, (b) $\Omega_s/2 \leqslant B_{E,n} < N\Omega_s/2$, (c) $B_{E,n} \geqslant N\Omega_s/2$.

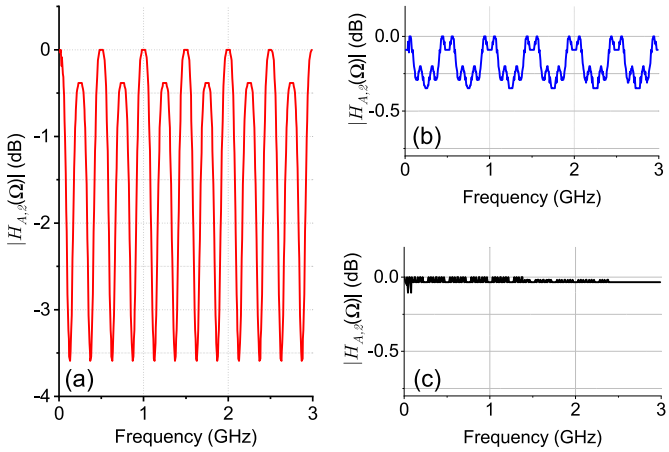

Fig. 5. The simulated $|H_{A,2}(\Omega)|$ in a 2-channel TIPADC when (a) $B_{E,2} = 100$ MHz, (b) $B_{E,2} = 135$ MHz, (c) $B_{E,2} = 2$ GHz.

$P'_{S,n}(k\Omega_s)$. Fig. 4 illustrates $H_{A,n}(\Omega)$ of a 4-channel TIPADC within the bandwidth of $H_M(\Omega)$ and $P_S(\Omega)$. For simplicity and not losing generality, we assume $H'_{E,n}(\Omega)$ has a rectangular magnitude response, and both $H'_{E,n}(\Omega)$ and $P_S(\Omega)$ have zero phase responses. When the bandwidth of $H'_{E,n}(\Omega)$, $B_{E,n}$, is less than $\Omega_s/2$, $H_{A,n}(\Omega)$ is composed of isolated duplicates of $H'_{E,n}(\Omega)$ with an interval of Ω_s due to the intrachannel crosstalk [7]. The magnitudes and phases of the duplicates have a periodicity of $N\Omega_s$ due to the interchannel crosstalk. As $\Omega_s/2 \leqslant B_{E,n} < N\Omega_s/2$, the adjacent duplicates of different magnitudes and phases would overlap with each other, which results in a continuous shape of $|H_{A,n}(\Omega)|$ with a periodicity of $N\Omega_s$ and crests locating at $kN\Omega_s$. In this case, there is no intrachannel crosstalk [7], and the periodicity is the effect of the interchannel crosstalk. As $B_{E,n} \geqslant N\Omega_s/2$, duplicates with the same magnitudes and phases, which have a periodicity of $N\Omega_s$, would overlap with each other and form a flat $|H_{A,n}(\Omega)|$. This indicates that neither of the crosstalks affects $H_{A,n}(\Omega)$. Now the bandwidth of $H_{A,n}(\Omega)$ is decided by $H_M(\Omega)$ as well as $P_S(\Omega)$.

Fig. 5 shows the magnitude responses of channel 2 under different $B_{E,n}$ in a 2-channel TIPADC simulated by VPItransmissionMaker Optical Systems. In the simulation, the repetition rate of optical pulses is 250 M/s, the channel intervals of WDMs are 200 GHz, and each channel has a shape of 2-order Gaussian function and a bandwidth of 150 GHz. 2-order Butterworth lowpass filters (LPF) with bandwidths of 100 MHz, 135 MHz and 2 GHz are applied after photodetection in channel 2, respectively. As shown in Fig. 5, both $|H_{A,2}(\Omega)|$ in (a) and (b) have a periodicity of 500 MHz ($2\Omega_s$), while in Fig. 5(c) it becomes flat. The 500 MHz-periodicity of $|H_{A,2}(\Omega)|$ is caused by the interchannel crosstalk in the 2-channel TIPADC with a single channel sampling rate of 250 M/s. Just as indicated by the above theoretical analysis, there exist ripples in Fig. 5(a) and (b) since 100 MHz and 135 MHz are less than $N\Omega_s/2$ (250 MHz). The ripples are flattened in Fig. 5(c) as 2 GHz is larger than $N\Omega_s/2$, duplicates of the same magnitudes and phases are able to overlap with each other. We can also see that $|H_{A,2}(\Omega)|$ in Fig. 5(a) is composed of isolated duplicates of $H'_{E,2}(\Omega)$ while in Fig. 5(b) it becomes continuous. This is because the adjacent duplicates with $B_{E,2}$ of 100 MHz are too narrow to overlap with each other, while the adjacent duplicates with $B_{E,2}$ of 135 MHz are broad enough to overlap with each other and form a continuous $|H_{A,2}(\Omega)|$ [7].

A 4-channel TIPADC is simulated and the magnitude responses of channel 2 under different $B_{E,n}$ are shown in Fig. 6. In this case, both $|H_{A,2}(\Omega)|$ in (a) and (b) have a periodicity of 1 GHz ($4\Omega_s$), while in (c) it becomes flat. The 1 GHz-periodicity

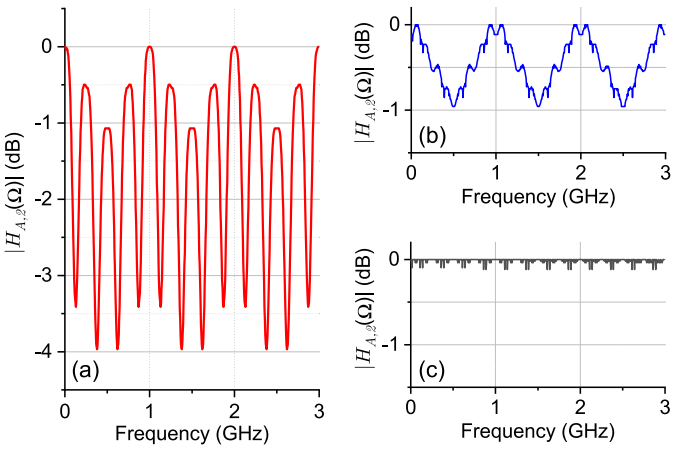

Fig. 6. The simulated $|H_{A,2}(\Omega)|$ in a 4-channel TIPADC when (a) $B_{E,2} =$ 100 MHz, (b) $B_{E,2} = 135$ MHz, (c) $B_{E,2} = 2$ GHz.

of $|H_{A,2}(\Omega)|$ is caused by the interchannel crosstalk in the 4-channel TIPADC. $|H_{A,2}(\Omega)|$ in Fig. 6(a) is composed of isolated duplicates of $H'_{E,2}(\Omega)$ while in Fig. 6(b) it becomes continuous. The ripples in Fig. 6(a) and (b) are flattened in Fig. 6(c) due to the large $B_{E,2}$ of 2 GHz.

From Fig. 5, Fig. 6 and (5), it can be seen that when $B_{E,n} < \Omega_s/2$, the magnitudes of signals at $k\Omega_s$ are determined by only one weighted duplicate of $H'_{E,n}(\Omega)$, which means that the interchannel-crosstalk-affected $\Gamma_n(k\Omega_s)$ can easily be identified. In the case, an upper limit of interchannel crosstalk can be analyzed relative to the ENOB of the used EADC. Take channel 1 of a 2-channel TIPADC as an example. When there is interchannel crosstalk, the difference between the maximum and minimum amplitudes of the analog signal at $k\Omega_s (k \in Z)$ can be expressed as:

$$\begin{aligned}&\Delta Amp\\&= \max\{Amp(k\Omega_s)\} - \min\{Amp(k\Omega_s)\}\\&= \frac{1}{\pi}\max\left\{|H_{A,1}(k\Omega_s)|\right\} - \frac{1}{\pi}\min\left\{|H_{A,1}(k\Omega_s)|\right\},\end{aligned} \quad (10)$$

where $Amp(k\Omega_s)$ denotes the amplitude of the analog signal of $k\Omega_s$ carried by the electrical pulse train before quantization. To ignore the effect of interchannel crosstalk relative to quantization noise, the maximum and minimum amplitudes of the analog signal at $k\Omega_s$ should be quantized to the same level, just as the case without interchannel crosstalk. Since the frequency response of channel without mismatch has the maximum magnitude at $2k\Omega_s$, we assume that the modulated part of the electrical pulse train for the modulating signal at this frequency is quantized at the full scale of the EADC, according to the most common configuration in practice, i.e., the full-scale range (FSR) is $2Amp(2k\Omega_s)$. In the case, we have:

$$\Delta Amp \leqslant \frac{1}{2}\,\mathrm{LSB} \Rightarrow \frac{\gamma_{1,2}}{\gamma_{1,1}} \leqslant \frac{1}{2^{b+1}-3}. \quad (11)$$

where $\mathrm{LSB} = \mathrm{FSR}/(2^b - 1)$, is the least significant bit and b is the ENOB of the EADC.

For example, when $b = 12$ bits, $\gamma_{1,2}$ should be less than $0.00012\gamma_{1,1}$ to ignore the effect of interchannel crosstalk. When (11) is satisfied, all the magnitudes of duplicates are the same in $|H_{A,1}(\Omega)|$. With the increase of $B_{E,1}$, the effect of the interchannel crosstalk is still negligible. When $N > 2$, the frequency position of duplicates with the smallest magnitude is unsure unless the exact values of $\gamma_{n,m}$ are given, then a judgment for the level of the interchannel crosstalk can be presented according to (10).

B. Channel Response With Channel Mismatch

In practical time-interleaved analog-to-digital converters (TIADCs), there are offset, gain, and time mismatches between different channels [12]–[16]. For TIPADCs, in addition to the mismatches caused by backend-EADCs and transmission paths, which are similar to those in TIEADCs, there are mismatches introduced by optical devices like MZM, Erbium-doped optical fiber amplifier (EDFA), WDMs, photodetectors (PDs) and so on. Channel mismatches interfere with the interleaving of multiple channels and result in spectral spurs in the output, which degrade the system's SNR, SFDR, and ENOB [17], [18].

When taking into consideration the mismatches, the model of channel response could be updated. Offset mismatch does not affect $|H_{A,n}(\Omega)|$ according to (2). Gain mismatch can be taken into account by changing $\gamma_{n,m}$ and $P_{A,n}$ numerically, whose effects on $|H_{A,n}(\Omega)|$ have been discussed in subSection II-A. Time mismatch can happen both in $d_{P,n}$ and $d_{E,n}$. $d_{E,n}$ only affects the sample position on the modulated electrical pulses, and its mismatch has the similar effect as gain mismatch [18].

Mismatch of $d_{P,n}$ will affect the sample position on the RF signal. For a mismatched $d_{P,m}$ which is composed of an ideal $\tilde{d}_{P,m}$ and an error Δt_m, we have:

$$\Gamma_n(\Omega) = \sum_{m=1}^{N} \gamma_{n,m} e^{-j\Omega\tilde{d}_{p,m}} e^{-j\Omega\Delta t_m}, \quad (12)$$

and:

$$\begin{cases} |\Gamma_n(k\Omega_s)| \neq |\Gamma_n(k\Omega_s + N\Omega_s)| \\ |\Gamma_n(k\Omega_s)| \leqslant \Gamma_n(0) \\ \arg[\Gamma_n(k\Omega_s)] \neq \arg[\Gamma_n(k\Omega_s + N\Omega_s)] \\ \arg[\Gamma_n(0)] = 0. \end{cases} \quad (13)$$

Equation (13) indicates that both $|\Gamma_n(k\Omega_s)|$ and $\arg[\Gamma_n(k\Omega_s)]$ lose the periodicity compared with (9), but still reach the maximum $|\Gamma_n(0)|$ and 0 at the zero frequency, respectively.

A 2-channel TIPADC with $\Delta t_2 = 0.2$ ns and different $B_{E,2}$ is simulated and the corresponding $|H_{A,2}(\Omega)|$ are shown in Fig. 7. Other simulation parameters are the same as those in Fig. 5. As shown in Fig. 7, when $B_{E,2} = 100$ MHz $< \Omega_s/2$, $|H_{A,2}(\Omega)|$ is composed of duplicates of $H'_{E,2}(\Omega)$ with an interval of 250 MHz, but the magnitudes of duplicates are aperiodic as each duplicate is disturbed by Δt_m. When $\Omega_s/2 \leqslant B_{E,2} < N\Omega_s/2$, adjacent duplicates of 250 MHz-interval overlap with each other and form a continuous but aperiodic $|H_{A,2}(\Omega)|$. When $B_{E,2} =$ 2 GHz $\geqslant N\Omega_s/2$, for each RF signal frequency, $H_{A,2}(\Omega)$ is composed of so many duplicates of $H'_{E,2}(\Omega)$, each with different

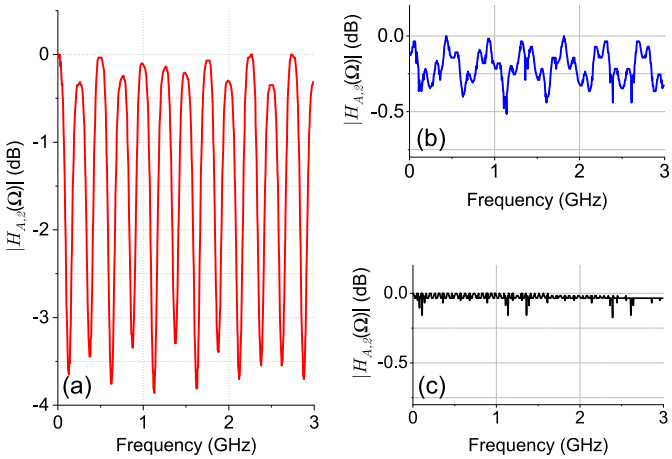

Fig. 7. The simulated $|H_{A,2}(\Omega)|$ in a 2-channel TIPADC with time mismatch when (a) $B_{E,2} = 100$ MHz, (b) $B_{E,2} = 135$ MHz, (c) $B_{E,2} = 2$ GHz.

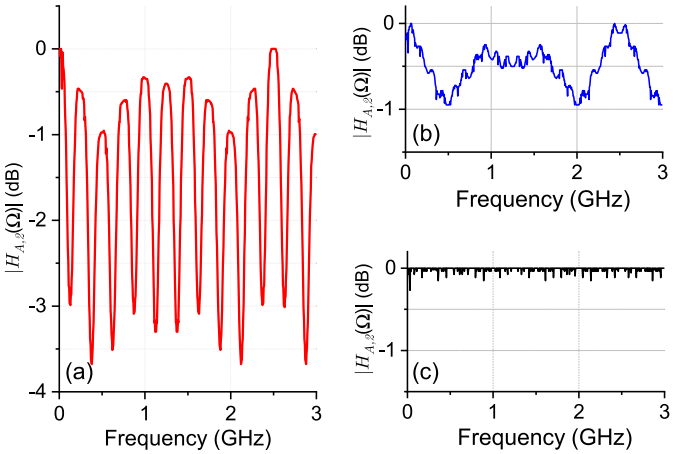

Fig. 8. The simulated $|H_{A,2}(\Omega)|$ in a 4-channel TIPADC with time mismatch when (a) $B_{E,2} = 100$ MHz, (b) $B_{E,2} = 135$ MHz, (c) $B_{E,2} = 2$ GHz.

magnitudes and phases, that the aperiodicity is weakened with the large $B_{E,2}$. As a result, $|H_{A,2}(\Omega)|$ is nearly flat.

A 4-channel TIPADC with $\Delta t_2 = 0.2$ ns and different $B_{E,2}$ is simulated and the corresponding $|H_{A,2}(\Omega)|$ are shown in Fig. 8. Other simulation parameters are the same as those in Fig. 6. Similar to Fig. 7, when $B_{E,2} = 100$ MHz $< \Omega_s/2$, $|H_{A,2}(\Omega)|$ is composed of duplicates of $H'_{E,2}(\Omega)$ with an interval of 250 MHz, but the magnitudes of duplicates are aperiodic. When $\Omega_s/2 \leqslant B_{E,2} < N\Omega_s/2$, adjacent duplicates of 250 MHz-interval overlap with each other and form a continuous but aperiodic $|H_{A,2}(\Omega)|$. When $B_{E,2} = 2$ GHz $\geqslant N\Omega_s/2$, $|H_{A,2}(\Omega)|$ is nearly flat.

As analyzed above, for a signal of $k\Omega_s$ being digitized by a TIPADC with interchannel crosstalk, there is amplitude difference between the outputs in the cases with and without time mismatch. In order to ignore the effect of interchannel crosstalk relative to quantization noise, the difference (denoted as $\Delta Amp'_n$) should be submerged in quantization noise. Denoting the frequency response of channel n in the case with and without time mismatch as $H^1_{A,n}(k\Omega_s)$ and $H^0_{A,n}(k\Omega_s)$, respectively. Denoting $\Gamma^1_n(k\Omega_s)$ and $\Gamma^0_n(k\Omega_s)$ are $\Gamma_n(k\Omega_s)$ corresponding to the system with and without time mismatch, respectively. The amplitude of the analog signal of Ω carried by electrical pulse train before quantization in the case with and without time mismatch is denoted as $Amp^1_n(\Omega)$ and $Amp^0_n(\Omega)$ for channel n, respectively. Take a 2-channel TIPADC as an example. Within the bandwidth of the modulator and the optical pulse, when $B_{E,n} < \Omega_s/2$, $\Delta Amp'_n(k\Omega_s)$ is:

$$\begin{aligned}\Delta Amp'_n(k\Omega_s) &= \left|Amp^1_n(k\Omega_s) - Amp^0_n(k\Omega_s)\right| \\ &= \frac{1}{\pi}\left||H^1_{A,n}(k\Omega_s)| - |H^0_{A,n}(k\Omega_s)|\right| \\ &= \frac{\alpha P'_{A,n}}{2\pi T_s}\left|H_M(k\Omega_s)P_S(k\Omega_s)H_{E,n}(k\Omega_s)\right| \\ &\quad \times \left||\Gamma^1_n(k\Omega_s)| - |\Gamma^0_n(k\Omega_s)|\right|, \end{aligned} \tag{14}$$

Considering that $|H^0_{A,1}(2\ \mathrm{k}\Omega_s)|$ has the maximum magnitude, the modulated part of the electrical pulse train in a system without time mismatch is assumed to be quantized at full scale when the modulating signal has a frequency of $2k\Omega_s$. In the configuration, for channel 1, i.e., $\gamma_{1,1} = 1$, in order to ignore the effects of the time mismatch relative to the quantization noise, we should have:

$$\begin{aligned}&\Delta Amp'_1(k\Omega_s) \leqslant \frac{1}{2}\mathrm{LSB} \\ &\Rightarrow \left||\Gamma^1_1(k\Omega_s)| - |\Gamma^0_1(k\Omega_s)|\right| \leqslant \frac{1+\gamma_{1,2}}{2^b - 1}, \end{aligned} \tag{15}$$

where b is the ENOB of the EADC. (15) guarantees that $Amp^1_1(2k\Omega_s)$ is not less than the upmost decision level, thus $Amp^0_1(2k\Omega_s)$ and $Amp^1_1(2k\Omega_s)$ are both quantized to the upmost quantization step of the EADC. As for the frequency of $(2k+1)\Omega_s$, the values of $Amp^0_1[(2k+1)\Omega_s]$ and $Amp^1_1[(2k+1)\Omega_s]$ are both uncertain, (15) can only guarantee that the difference between the quantized results of them is not more than one quantization step. Take channel 1 as reference channel which has no time mismatch, i.e., $\Delta t_1 = 0$. According to (12),

$$\begin{aligned}&\left||\Gamma^0_1(k\Omega_s)| - |\Gamma^1_1(k\Omega_s)|\right| \\ &= \left|\sqrt{1+\gamma^2_{1,2}+2\gamma_{1,2}e^{-j\pi k}\cos\left(\frac{2\pi k\Delta t_2}{T_s}\right)}\right. \\ &\quad \left. - \left(1+\gamma_{1,2}e^{-j\pi k}\right)\right|. \end{aligned} \tag{16}$$

From (15) and (16), we have the upper limit of $|\Delta t_2|$:

$$\begin{aligned}&\max\{|\Delta t_2|\} = \\ &\begin{cases} k = 0, \pm 2, \pm 4, \ldots : \\ \frac{T_s}{2\pi k}\arccos\left\{\frac{1}{2\gamma_{1,2}}\left[(1+\gamma_{1,2}) - \frac{1+\gamma_{1,2}}{2^b-1}\right]^2 - \frac{1+\gamma^2_{1,2}}{2\gamma_{1,2}}\right\}, \\ k = \pm 1, \pm 3, \pm 5, \ldots : \\ \frac{T_s}{2\pi k}\arccos\left\{\frac{1+\gamma_{1,2}}{2\gamma_{1,2}} - \frac{1}{2\gamma_{1,2}}\left[(1-\gamma_{1,2}) + \frac{1+\gamma^2_{1,2}}{2^b-1}\right]^2\right\}. \end{cases} \end{aligned} \tag{17}$$

below which the amplitude disturbance caused by the time mismatch can be ignored relative to quantization noise in the

TABLE I
$\max\{|\Delta t_2|\}$ FOR DIFFERENT FREQUENCY RANGES

kf_s(GHz)	0.5	1.5	2.5	3.5	...	5
$\max\{\|\Delta t_2\|\}$(ps)	12.254	4.085	2.451	1.751	...	1.670

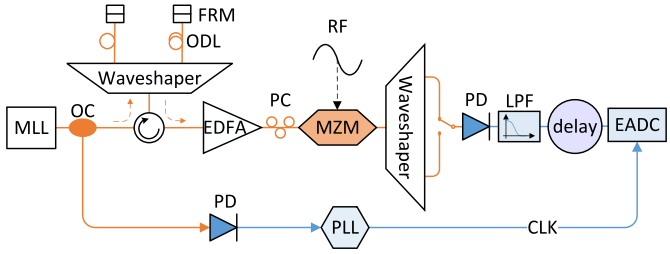

Fig. 9. Experiment setup. MLL: Mode-Locked Laser; OC: Optical Coupler; ODL: Optical Delay Line; FRM: Faraday Rotator Mirror; EDFA: Erbium-Doped Optical Fiber Amplifier; PC: Polarization Controller; MZM: Mach-Zehnder Modulator; PD: Photodiode; LPF: Low Pass Filter; PLL: Phase-Locked Loop.

frequency range of $[0, k\Omega_s]$. Table I illustrates the $\max\{|\Delta t_2|\}$ under different frequency ranges when the repetition rate of MLL is 100 MHz, $b = 12$ bits and $\gamma_{1,2} = 0.3$.

Although (11) is discussed without mismatch, the condition of (10) guarantees that (11) is the strictest acceptable constraint range of the interchannel crosstalk applicable for any time mismatch. This is because time mismatch disturbs $|H^0_{A,1}(k\Omega_s)|$ and results in $|H^1_{A,1}(k\Omega_s)|$, but $\max\{|H^1_{A,1}(k\Omega_s)|\} \leqslant \max\{|H^0_{A,1}(k\Omega_s)|\}$ and $\min\{|H^1_{A,1}(k\Omega_s)|\} \geqslant \min\{|H^0_{A,1}(k\Omega_s)|\}$. Under the constraint of (11), the interchannel crosstalk is small enough and the frequency response of a single channel is nearly independent of other channels, thus it is not affected by time mismatch.

III. EXPERIMENTS

We build a 2-channel TIPADC and the schematic is illustrated in Fig. 9. A passive mode-locked fiber laser (MLL) (Precision Photonics, FFL1560) generates a pulse train at a repetition rate of 36.456 MHz with an average power of 10 mW and a pulse width of 70 fs. The pulse train is split by an optical coupler (OC). One part is used to drive the phase-locked loop (PLL) to generate a clock for digitization. The repetition rate of the other part is doubled by a circulator, a waveshaper (Finisar, 16000), tunable delay lines and 2 Faraday rotator mirrors (FRMs). The waveshaper is used as a channel bandwidth- and interval-tunable WDM. After amplified by an EDFA, the pulse train is modulated in an MZM by RF signal. The MZM has a half-wave voltage of about 4.5 V and is biased at quadrature. The power of the RF signal is set to be 0 dBm to reduce the nonlinearity. The modulated pulse train is demultiplexed by another waveshaper (Finisar, 4000S) which has the same channel configuration as the former one. Finally, the demultiplexed pulse train of each channel, which has a repetition rate of 36.456 MHz, is detected by the same PD, filtered by an LPF, and sampled as well as digitized by an ADC/digitizer (Keysight, M9703 A).

Both 2 channels are of the 2-order Gaussian function shapes with a bandwidth of 200 GHz and locate at 192.2 THz and 192.4 THz, respectively, as shown in Fig. 10(a). The pulse trains of 2 channels after the PD are shown in Fig. 10(b). In each channel, crosstalk pulses insert between the main pulse train. The lower amplitude of the main pulse train in channel 2 compared with that of channel 1 is due to the larger attenuation of the corresponding FRM, which means the relative effect of the interchannel crosstalk in channel 2 is more evident than that in channel 1.

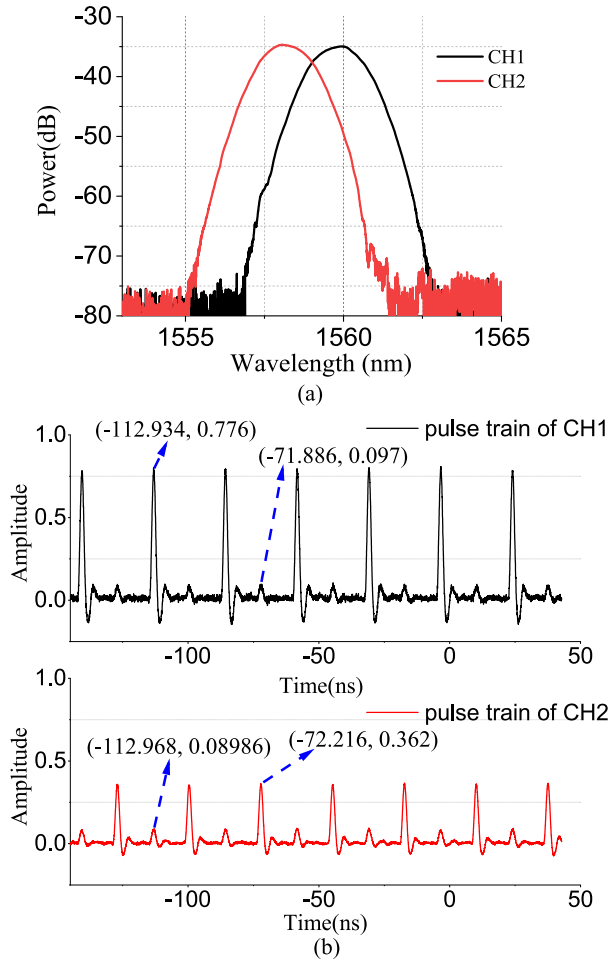

Fig. 10. (a) Spectrum of 2 channels, (b) Pulse trains of 2 channels.

The normalized magnitude responses of 2 channels under 3 backend bandwidths without time mismatch are shown in Fig. 11 and Fig. 12. When LPFs bandwidth of 14 MHz and 24.5 MHz are applied respectively, since they have the narrowest bandwidths compared with all the other running electronic devices from the photodiode to the EADC, the backend bandwidths approximate to the bandwidths of applied LPFs, respectively. When there is no LPF applied, the backend bandwidth is limited to 1.2 GHz by the EADC. As $B_{E,n} = 14$ MHz $< \Omega_s/2$, both $|H_{A,n}(\Omega)|$ of channel 1 and 2 are composed of isolated duplicates of $H'_{E,n}(\Omega)$ with alternate magnitudes and an interval of 36.456 MHz, and have a periodicity of 72.912 MHz. As the relative interchannel crosstalk in channel 2 is severer than that in channel 1, the magnitude difference between the duplicates is larger in channel 2. When $B_{E,n} = 24.5$ MHz $\geqslant \Omega_s/2$ (18.228 MHz) but less than

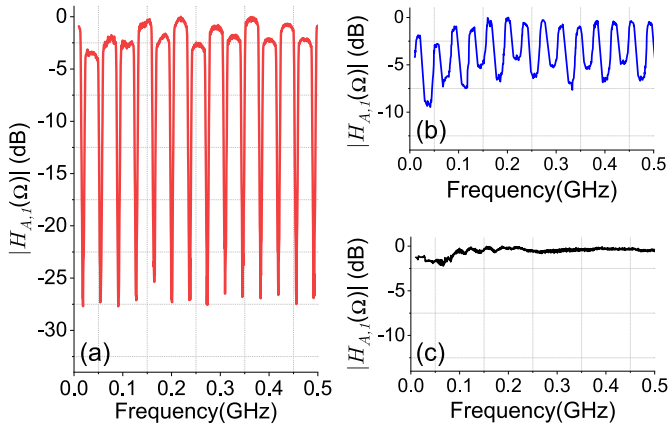

Fig. 11. $|H_{A,1}(\Omega)|$ with $B_{E,1}$ of: (a) 14 MHz, (b) 24.5 MHz, (c) 1.2 GHz.

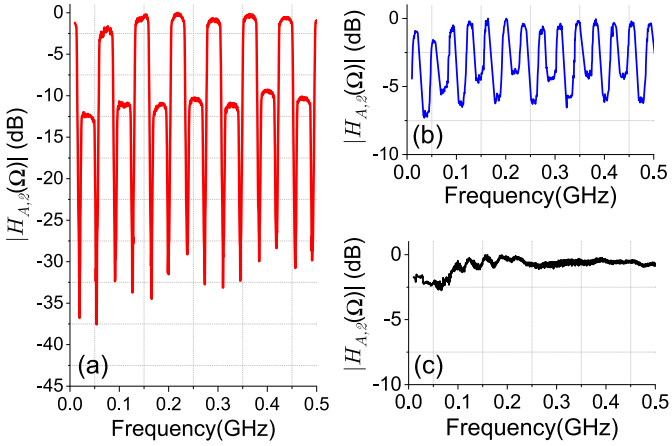

Fig. 12. $|H_{A,2}(\Omega)|$ with $B_{E,2}$ of: (a) 14 MHz, (b) 24.5 MHz, (c) 1.2 GHz.

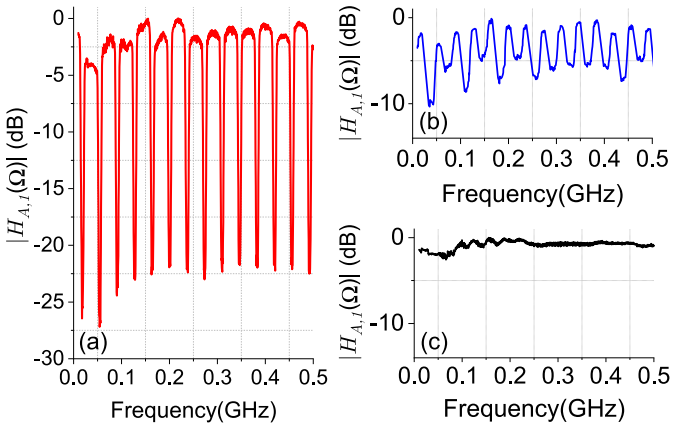

Fig. 13. $|H_{A,1}(\Omega)|$ with time mismatch and $B_{E,1}$ of: (a) 14 MHz, (b) 24.5 MHz, (c) 1.2 GHz.

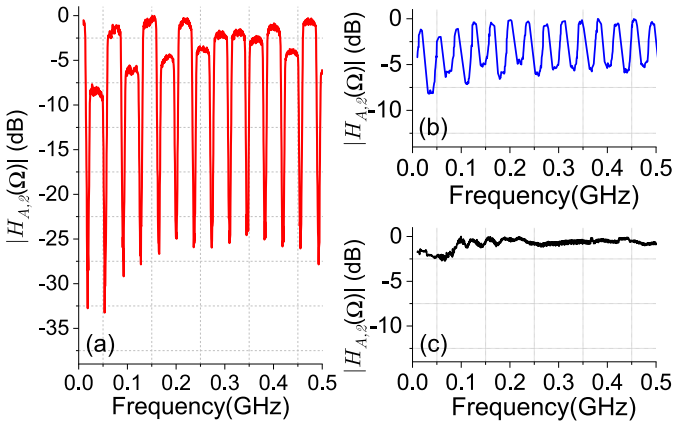

Fig. 14. $|H_{A,2}(\Omega)|$ with time mismatch and $B_{E,2}$ of: (a) 14 MHz, (b) 24.5 MHz, (c) 1.2 GHz.

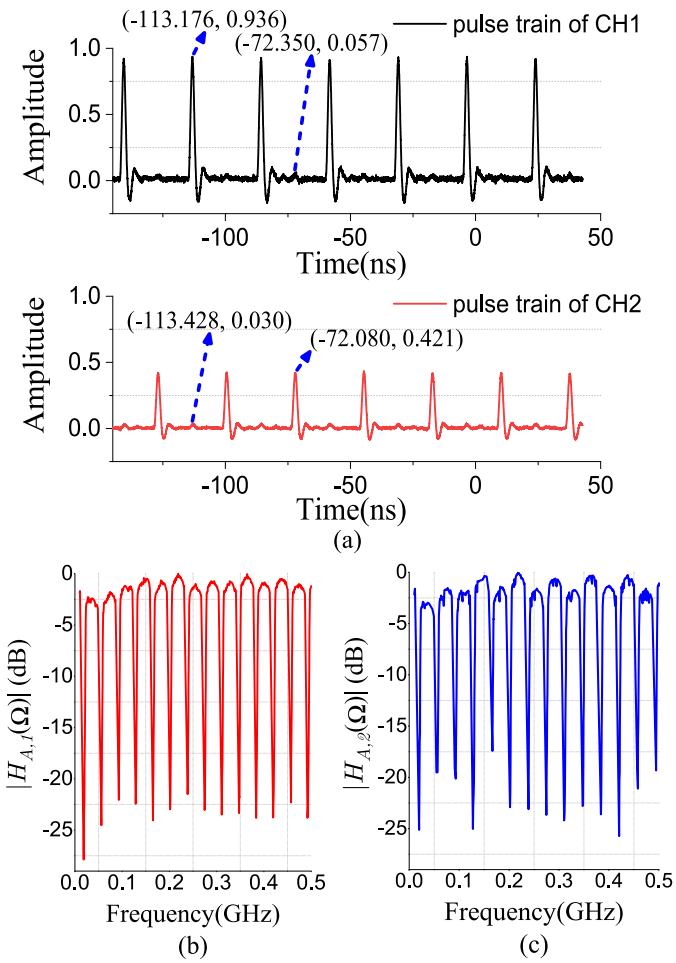

Fig. 15. (a) Pulse trains of 2 channels without time mismatch, (b) $|H_{A,1}(\Omega)|$ without time mismatch, (c) $|H_{A,2}(\Omega)|$ without time mismatch.

$N\Omega_s/2$ (36.456 MHz), adjacent duplicates of 36.456 MHz overlap with each other and result in peaks at the two sides of each duplicate locating at $\Omega_s/2 + k\Omega_s$. The troughs of the magnitude responses locating at $k\Omega_s$ are still magnitude-alternately and the magnitude responses have a periodicity of 72.912 MHz. When $B_{E,n} = 1.2\ \text{GHz} \geqslant N\Omega_s/2$, duplicates with the same magnitudes and phases overlap with each other and form a nearly flat $|H_{A,n}(\Omega)|$, which is mainly determined by the non-ideal response of the system. This non-ideal response also disturbed the periodicity in Fig. 11(a) and (b) in low frequency.

The channel magnitude responses with time mismatch are measured and shown in Fig. 13 and Fig. 14. Time mismatch of about 0.8 ns is introduced by adjusting the tunable delay line in

channel 2. Compared with Fig. 11 and Fig. 12, when $B_{E,n} =$ 14 MHz and 24.5 MHz, $|H_{A,n}(\Omega)|$ lose the periodicity of 72.912 MHz since the magnitude of each duplicate is disturbed by the time mismatch. When $B_{E,n} = 1.2\ \text{GHz} \geqslant N\Omega_s/2$, duplicates are so broad that at each frequency $|H_{A,n}(\Omega)|$ is composed of many duplicates with different magnitudes and phases, resulting in nearly flat magnitude responses for both channel 1 and channel 2.

Fig. 15(a) shows the pulse trains of 2 channels after PD and the corresponding channel magnitude responses when the shapes of 2 channels are 4-order Gaussian function. Both 2 channels still have a bandwidth of 200 GHz and locate at 192.2 THz and 192.4 THz, respectively. There is no time mismatch introduced intentionally in the system. Compared with Fig. 10(b), the lower amplitude of crosstalk pulses indicates that given the same bandwidth and channel interval, 4-order Gaussian function shape performs better in resisting the interchannel crosstalk. Accordingly, the magnitude difference between the duplicates of $H_{E,n}^{'}(\Omega)$ is much smaller in both 2 channels when backend bandwidth is 14 MHz compared with Fig. 11(a) and Fig. 12(a).

IV. Conclusion

We establish the model of channel response including interchannel and intrachannel crosstalks for TIPADCs. The effects of crosstalks on the channel magnitude responses in the cases with and without mismatch are analyzed under different backend bandwidths. The upper limit of crosstalk and time mismatch are investigated by comparing with quantization noise. 2- and 4-channel TIPADCs with and without time mismatch are simulated under different backend bandwidths. The results are consistent with the theoretical analysis. The channel magnitude responses of a 2-channel TIPADC system are experimentally measured under different backend bandwidths, interchannel crosstalk levels, time mismatches and channel shapes, respectively. The experimental results verify the theory and simulation. When interleaving multiple channels, crosstalks will lead to frequency response mismatch. Based on the response of the single channel, the amplitude and phase of the output signal and the interleaving spurs can be obtained for any RF input signal.

Appendix

This appendix presents the derivation of the channel response in (5).

$$
\begin{aligned}
&H_{A,n}(\Omega) \\
&\quad = -\frac{1}{2}\alpha H_M(\Omega) \times \left\{ \frac{1}{2\pi} H_{E,n}(\Omega) e^{-j\Omega d_{E,n}} \right. \\
&\qquad \left. * \left[P_{A,n} \frac{2\pi}{T_s} \sum_{k=-\infty}^{\infty} P_{S,n}^{'}(k\Omega_s)\delta(-\Omega - k\Omega_s) \right] \right\} \\
&\quad = -\frac{\alpha P_{A,n}}{2T_s} H_M(\Omega) \left\{ H_{E,n}(\Omega) e^{-j\Omega d_{E,n}} \right. \\
&\qquad \left. * \left[\sum_{k=-\infty}^{\infty} P_S^{'}(k\Omega_s)\,\delta(\Omega + k\Omega_s) \right] \right\} \\
&\quad = -\frac{\alpha P_{A,n}}{2T_s} H_M(\Omega) \left[\sum_{k=-\infty}^{\infty} P_S^{'}(k\Omega_s) \right. \\
&\qquad \left. \times\ H_{E,n}(\Omega + k\Omega_s) e^{-j(\Omega + k\Omega_s)d_{E,n}} \right] \\
&\quad = -\frac{\alpha P_{A,n}}{2T_s} H_M(\Omega) \sum_{k=-\infty}^{\infty} P_S^{'}(k\Omega_s) H_{E,n}^{'}(\Omega + k\Omega_s).
\end{aligned}
\tag{18}
$$

References

[1] J. A. Bell, M. C. Hamilton, D. A. Leep, T. D. Moran, H. F. Taylor, and Y. Lee, "Extension of electronic a/d converters to multi-gigahertz sampling rates using optical sampling and demultiplexing techniques," in *Proc. 33rd Asilomar Conf. Signals, Syst. Comput.*, 1989, pp. 289–293.

[2] T. R. Clark, J. U. Kang, and R. D. Esman, "Performance of a time- and wavelength-interleaved photonic sampler for analog-digital conversion," *IEEE Photon. Technol. Lett.*, vol. 11, no. 9, pp. 1168–1170, Sep. 1999.

[3] P. W. Juodawlkis *et al.*, "505-ms/s photonic analog-to-digital converter," in *Proc. Tech. Dig. Summaries Papers Presented Conf. Lasers Electro-Opt. Postconference Tech. Dig. (IEEE Cat. No.01CH37170)*, 2001, pp. 63–64.

[4] G. C. Valley, "Photonic analog-to-digital converters," *Opt. Express*, vol. 15, no. 5, pp. 1955–1982, 2007.

[5] R. C. Williamson, P. W. Juodawlkis, J. L. Wasserman, G. E. Betts, and J. C. Twichell, "Effects of crosstalk in demultiplexers for photonic analog-to-digital converters," *J. Lightw. Technol.*, vol. 19, no. 2, pp. 230–236, Feb. 2001.

[6] K. Furusawa, I. Morohashi, N. Sekine, and I. Hosako, "A photonic assisted analog-to-digital converter (p-adc) based on a 10 ghz frequency comb source," in *Proc. Prog. Electromagn. Res. Symp. Fall*, 2017, pp. 2759–2764.

[7] F. Su, G. Wu, L. Ye, R. Liu, X. Xue, and J. Chen, "Effects of the photonic sampling pulse width and the photodetection bandwidth on the channel response of photonic adcs," *Opt. Express*, vol. 24, no. 2, pp. 924–934, 2016.

[8] H. Gevorgyan, K. A. Qubaisi, M. S. Dahlem, and A. Khilo, "Silicon photonic time-wavelength pulse interleaver for photonic analog-to-digital converters," *Opt. Express*, vol. 24, no. 12, pp. 13 489–13 499, 2016.

[9] E. Krune, B. Krueger, L. Zimmermann, K. Voigt, and K. Petermann, "Comparison of the jitter performance of different photonic sampling techniques," *J. Lightw. Technol.*, vol. 34, no. 4, pp. 1360–1367, Feb. 2016.

[10] H. A. Jamal and S. Ghafoor, "A novel time and wavelength interleaved optical pulsed signal for a high resolution photonic analogue to digital converter," *Opt. Quantum Electron.*, vol. 50, no. 2, pp. 98(1–10), 2018.

[11] J. D. McKinney and K. J. Williams, "Sampled analog optical links," *IEEE Trans. Microw. Theory Techn.*, vol. 57, no. 8, pp. 2093–2099, Aug. 2009.

[12] F. Daihong, K. C. Dyer, S. H. Lewis, and P. J. Hurst, "A digital background calibration technique for time-interleaved analog-to-digital converters," *IEEE J. Solid-State Circuits*, vol. 33, no. 12, pp. 1904–1911, Dec. 1998.

[13] K. C. Dyer, D. H. Fu, S. H. Lewis, and P. J. Hurst, "An analog background calibration technique for time-interleaved analog-to-digital converters," *IEEE J. Solid-State Circuits*, vol. 33, no. 12, pp. 1912–1919, Dec. 1998.

[14] J. Huawen and E. K. F. Lee, "A digital-background calibration technique for minimizing timing-error effects in time-interleaved adcs," *IEEE Trans. Circuits Syst. II: Analog Digit. Signal Process.*, vol. 47, no. 7, pp. 603–613, Jul. 2000.

[15] C. Vogel and H. Johansson, "Time-interleaved analog-to-digital converters: Status and future directions," in *Proc. IEEE Int. Symp. Circuits Syst.*, 2006, pp. 3386–3389.

[16] J. Matsuno, T. Yamaji, M. Furuta, and T. Itakura, "All-digital background calibration technique for time-interleaved adc using pseudo aliasing signal," *IEEE Trans. Circuits Syst. I: Regular Papers*, vol. 60, no. 5, pp. 1113–1121, May 2013.

[17] G. Yang, W. Zou, L. Yu, K. Wu, and J. Chen, "Compensation of multichannel mismatches in high-speed high-resolution photonic analog-to-digital converter," *Opt. Express*, vol. 24, no. 21, pp. 24 061–24 074, 2016.

[18] Z. Jin, G. Wu, C. Wang, and J. Chen, "Mismatches analysis based on channel response and an amplitude correction method for time interleaved photonic analog-to-digital converters," *Opt. Express*, vol. 26, no. 14, pp. 17 859–17 871, 2018.

Cheng Wang was born in Shanxi, China, in 1995. He received the B.S. degree from Xidian University, Shaanxi, China, in 2016. He is currently working toward the Ph.D. degree in electronic science and technology with the State Key Laboratory of Advanced Optical Communication Systems and Networks, Department of Electronic Engineering, Shanghai Jiao Tong University, Shanghai, China. His research interests include digital signal processing and photonic analog-to-digital conversion.

Guiling Wu received the B.S. degree from the Harbin Institute of Technology, Harbin, China, in 1995 and the M.S. and Ph.D. degrees from the Huazhong University of Science and Technology, Wuhan, China, in 1998 and 2001, respectively. He is currently a Professor with the State Key Laboratory of Advanced Optical Communication Systems and Networks, Department of Electronic Engineering, Shanghai Jiao Tong University, Shanghai, China. His current research interests include photonic signal processing and transmission.

Zhengtao Jin was born in Henan, China, in 1993. He received the B.S. degree from the University of Electronic Science and Technology of China, Sichuan, China, in 2015. He is currently working toward the Ph.D. degree with the State Key Laboratory of Advanced Optical Communication Systems and Networks, Department of Electronic Engineering, Shanghai Jiao Tong University, Shanghai, China. His research interests include microwave photonics and photonic analog-to-digital conversion.

Jianping Chen received the B.S. degree from Zhejiang University, Hangzhou, China, in 1983 and the M.S. and Ph.D. degrees from Shanghai Jiao Tong University, Shanghai, China, in 1986 and 1992, respectively. He is currently a Professor with the State Key Laboratory of Advanced Optical Communication Systems and Networks, Department of Electronic Engineering, Shanghai Jiao Tong University. His research interests include photonic devices and signal processing, optical networking, and sensing optics. He is also a Principal Scientist of the 973 project in China.